PHOTOCHEMICALLY PATTERNED BILIARY STENTS WITH INTEGRATED PERMANENT MAGNETS AND DEFORMABLE ASSEMBLY FEATURES FOR WIRELESS MAGNETOELASTIC TISSUE GROWTH SENSING

Scott R. Green[1*], Mark T. Richardson[2], Farah A. Shariff[2], and Yogesh B. Gianchandani[1,2]
[1]Department of Mechanical Engineering, University of Michigan, Ann Arbor
[2]Department of Electrical Engineering and Computer Science, University of Michigan, Ann Arbor
*1301 Beal Ave., Ann Arbor, MI 48109; email greensr@umich.edu

Abstract: Sludge accumulation in biliary stents causes a loss of patency, leading to complications such as jaundice. We report batch-fabricated biliary stents with integrated magnetoelastic sensors for monitoring tissue growth. Integrated neodymium magnets bias the sensor and remove a source of measurement error. Paraffin mass loads up to 44.2 mg simulated tissue growth on 37.5x2 mm^2, 28 μm thick sensors. A resonant frequency shift from 58.81 kHz to 34.42 kHz was observed. The sensor provides a usable signal to the interrogation system if present within at least a 320 cm^3 volume adjacent to the interrogation coils.

Keywords: magnetostrictive, biliary sludge, bulk metal microstructures

I. INTRODUCTION

Stents are mesh tubular structures used to impart and maintain patency in a variety of vessels and ducts that have become constricted as a result of stenotic pathology. Though the act of implanting a stent relieves symptoms caused by the constriction, it also will elicit an immune response that results in the encapsulation of the foreign surfaces. This encapsulation may cause the duct to once again become occluded; this process is termed restenosis and is a risk associated with all stenting procedures.

An example of a stent application area – and the focus of this work – is the bile duct, which transports bile between the liver, gall bladder, pancreas, and small intestine. The constriction relieved by stent implantation is often due to pancreatitis, cholangitis, tumors, or gallstones. Restenosis can occur in an average of 4-5 months via formation of a bacterial matrix known as biliary "sludge" [1].

Current techniques for diagnosing a blockage are indirect and rely on detecting enzyme levels that may not increase until after the blockage is significant. As such, a direct method – such as that shown in Fig. 1 – would enable timely intervention and eliminate unnecessary procedures. We have previously reported on magnetoelastic wireless sensing of sludge accumulation utilizing externally applied AC interrogative and DC biasing magnetic fields [2]. The magnetic fields cause a magnetoelastic sensor integrated with the stent to resonate at a frequency that changes as local viscosity increases and as tissue accumulates. However, the resonant frequency is also dependent on the orientation of the applied DC biasing field (Fig. 2). Because the orientation of the interrogation equipment with respect to the sensor can vary on a test-to-test or patient-to-patient basis, a DC field emanating from this equipment could falsely shift the resonant frequency and result in an erroneous diagnosis. It is therefore desirable to integrate permanent magnets with the stent. This results in a fixed orientation between the field and the sensor, reducing a possible source of measurement error.

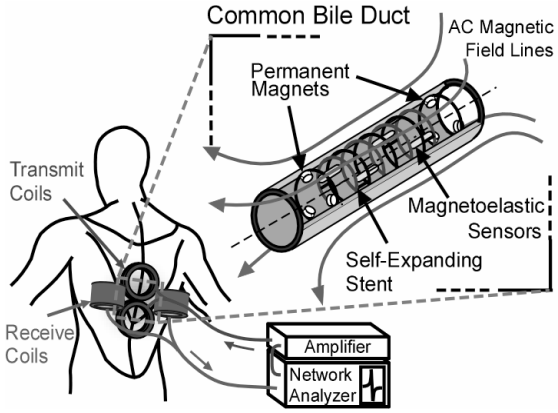

Fig. 1: Conceptual diagram of in-vivo magnetoelastic sensing of tissue growth for biliary stents. The inclusion of permanent magnets in the stent simplifies the external setup and reduces a significant source of signal amplitude and frequency variation.

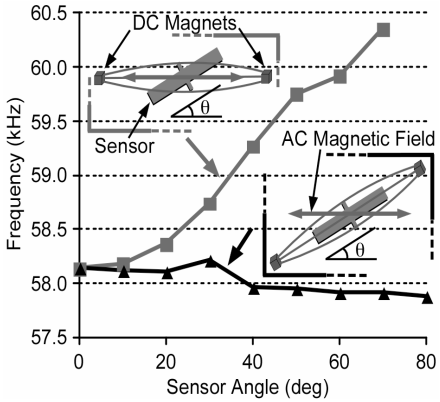

Fig. 2: The upper trace shows a large frequency shift of up to 2 kHz occurs when the relative DC field orientation varies. However, maintaining the orientation of the DC field to the sensor renders the resonant frequency insensitive to the AC field strength and orientation.

Our previous work has also shown the feasibility of micro-electro-discharge machining (μEDM) of cardiac stents in a planar manufacturing approach [3]. For the application detailed in this work, a planar approach is also warranted, making additional levels of integration and fabrication simplification possible by including mechanical features for sensor attachment and stent seam closure. To this end, the stents used in this work are batch fabricated using photochemical machining.

II. DESIGN AND FABRICATION

Permanent Magnets

The permanent magnets must be integrated in such a way as to provide a magnetic field of sufficient uniformity and magnitude to properly bias the sensor, yet also to minimally interfere with the expansion of the stent and allow an open lumen to be maintained. For the 12-37.5 mm long by 2-6 mm wide sensors used in this study, a bias field strength of 2.5-3 Oe is necessary for optimal signal amplitude. A conceptual schematic of an integration scheme is shown in Fig. 3. A finite element simulation was performed (Ansoft Maxwell 11.1) using two circumferential rings of six 0.8 mm thick by 1.6 mm diameter neodymium magnets. Simulation results show that this configuration can achieve sufficient field strength and uniformity for the needs of this design.

The majority of the reports on the use of rare-earth permanent magnets in biomedical implants are focused on intra-oral magnets for dentistry and orthodontic purposes. Though the intra-oral environment is not identical to that of the bile duct, these investigations do allow some conclusions to be drawn regarding the biocompatibility of rare-earth permanent magnets. The research notes that, although bare neodymium magnets are susceptible to corrosion in saliva – especially in the presence of bacteria – a parylene coating is effective in protecting against corrosion [4]. Additional research shows that the response of buccal mucosa (the lining of the cheeks and lips) exposed to a magnetized implant with 80-140 Oe field strength is negligibly different from the response of the same tissue exposed to a demagnetized implant [5]. These findings suggest that a passivated rare-earth magnet of the size and strength that we require does not pose a significant biocompatibility risk.

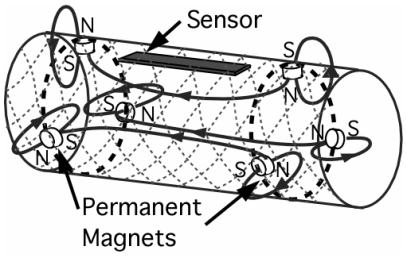

Fig. 3: Conceptual schematic of in-stent permanent magnet configuration and resulting field lines. The magnets are incorporated in the stent sidewall to maintain an open lumen. The magnets are located outside of the length of the sensor so that the sensor does not attach to the magnets during the stent expansion process. By orienting similar poles toward the center of the stent at either magnet ring location, stent expansion is unhindered by mutual attraction.

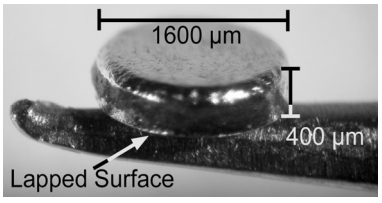

Fig. 4: Neodymium magnet lapped from 800µm to 400µm, on tip of tweezers.

As sensor length is reduced, the required bias field strength for optimal signal increases slightly. However, because a reduction in sensor length allows the circumferential rings of permanent magnets to be spaced more closely together along the length of the stent, a slightly stronger field can be provided by smaller magnets. For instance, a reduction in sensor length from 37.5 mm to 12.5 mm allows a reduction in magnet thickness from 800 μm to 400 μm. The thickness of the magnets was controlled by utilizing a lapping procedure with a diamond slurry (Fig. 4).

The permanent magnets can be attached to appropriate portions of the stent using a biocompatible adhesive or epoxy. For this preliminary work, a quick-setting epoxy was used to affix the magnets.

Stents

By utilizing the photochemical machining process, the designer is granted freedom to include assembly points at which the sensor can be attached. As noted in our previous work, it is important that the sensor is attached in such a way that contact between the sensor and the stent is limited. In view of this, the sensor attachment points in this work take the form of hooks (Fig. 5). Prior to attaching the sensor, the hooks are folded up so they stand out of plane. In this manner, the hooks act as not only an attachment point, but also as a stand-off that provides an operating gap between the sensor and the stent sidewall.

Commercial self-expanding stents (Boston Scientific) rely on elastic expansion of a woven metal mesh. The mesh consists of 10-15 small diameter (~100 μm) wires that are braided together in a tubular shape. This manufacturing process adds challenge to the inclusion of features that allow the attachment of sensors for enhanced functionality. An investigation into alternative stent fabrication approaches is thus warranted. For this work, stents are batch fabricated from planar 316L stainless steel foil patterned by photochemical machining (Fotofabrication Corp.). This process utilizes a laser-defined mask to lithographically

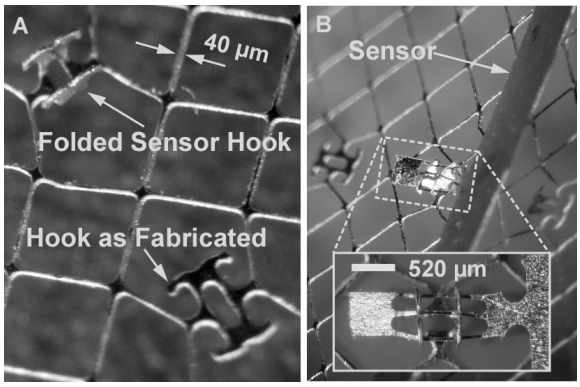

Fig. 5: A) Integrated sensor attachment points before folding out of the plane of the stent sidewall. B) Assembled sensor and stent at midlength. The attachment points also serve as standoffs to minimize contact-associated signal degradation.

pattern a laminated photoresist (PR) layer covering the base metal layer. The PR is developed and the unprotected metal is etched with a heated spray of etchant. For processing 316L stainless steel, a dry film PR (Accuimage, Kolon Ind.) and a ferric chloride etchant is used. For a 50μm thick foil, lateral feature sizes are as small as 33μm in this work, with external radii as small as 22 μm. Tolerances for the process are +/- 10% of the foil thickness.

Sensors

The magnetoelastic sensors are patterned from 28 μm thick planar Ni/Fe alloy foil (Metglas™ 2826MB) by μEDM [6]. The basic sensor shape is a beam of constant cross-section. The attachment feature on the sensor is an integrated clip at the beam mid-length. This clip is fabricated at the same time as the sensor using either serial or batch-mode μEDM [7]. In this work, the clip consists of three beams coupled at the ends (Fig. 5). This clip is aligned over the hooks on the stent and then brought into engagement with the hooks. As the engagement length increases, the outer beams are deflected over the hooks and eventually snap elastically back into place under the hooks. The middle beam remains on top of the hook and keeps the other beams engaged with the hooks. This arrangement keeps the clip and sensor at the top of the hook and away from the stent sidewall, as required.

Final Assembly

The sensor is attached and the permanent magnets are affixed while the stent remains in a planar state. In order to prop open the bile duct as intended, the planar stent must be shaped into a tube. The photochemical machining process allows for deformable mechanical features to be placed on the lateral edges of the planar stent. When the stent is rolled into a tubular shape, these mechanical features can be interlocked such that the tubular shape is maintained (Fig. 6). The mechanical features remain inside the tubular profile of the stent so they do no damage to the duct wall. The stent in its final assembly state is shown in Fig. 7.

III. MAGNETOELASTIC SENSOR MODELING

The effects of the dynamic biological environment on the sensor response are modeled in our previous work [2]. However, this model does not include any effects that justify the dependence of the resonant frequency on the bias field strength or orientation as shown in Fig. 2. To model this dependence, the "ΔE effect" is utilized, in which stiffness changes occur when magnetostrictive materials are exposed to DC magnetic fields [8]. Thus, the Young's modulus of the sensor varies with the applied DC magnetic field:

$$E = E_o + \phi(H_{DC}), \tag{1}$$

where E is the apparent Young's modulus of the sensor, E_o is the Young's modulus with zero bias, H_{DC} is the applied DC magnetic field strength, and ϕ is a generally nonlinear function relating the bias field strength to the incremental stiffness change. For the purposes of this work, H_{DC} varies over a relatively small range (0-4 Oe), and over this range ϕ can be represented as a proportional factor of around 21-31 GPa/Oe for Metglas™ 2826MB [11]. The zero-bias Young's modulus for this alloy is 100-110 GPa. With these values, we see that a change in bias field strength from

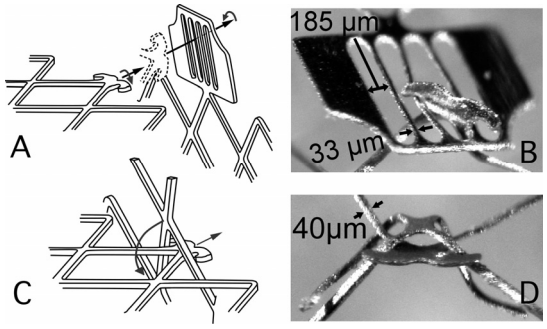

Fig. 6: A,B) Conceptual drawing and image of seam closure method 1. The hook is rotated 90 degrees and inserted through the slot. The hook returns to its as-fabricated orientation and resists disassembly. C,D) Conceptual drawing and image of method 2. The mesh on the opposite side of the seam acts as an alignment feature for the hook. The tines are then folded over.

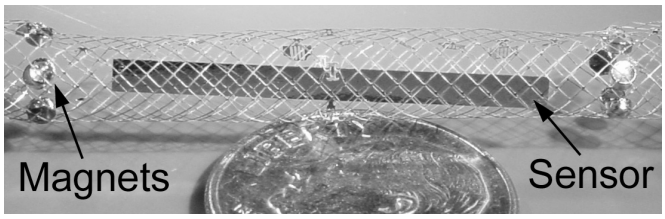

Fig. 7: Fully assembled device, shown with a US dime. The stent is 5.5mm in diameter. The sensor is 25x2mm^2, 28µm thick. The 12 magnets are 800µm thick and 1.6mm in diameter and attached with epoxy.

3 Oe to 2.7 Oe (a 10% decrease) results in a change in apparent Young's modulus from nominally 183 GPa to nominally 175.2 GPa (a 4.3% decrease). Finally, since the resonant frequency of the sensor is roughly proportional to the square root of the Young's modulus, a 2% shift in resonant frequency results. This analysis highlights the need to maintain a consistent bias field to reduce unwanted variability in the measurand.

IV. EXPERIMENTAL RESULTS

The test setup and experimental procedure used to measure the frequency response of the sensor in relevant conditions is nearly identical to that described in our previous work [2]. However, because this work integrates the permanent magnets with the stent and sensor, the permanent magnets that were previously outside the test vial are removed. The test vial and stent were placed within a 7.5 cm thick package of bovine tissue in order to simulate the signal attenuation due to the intervening tissue of the patient. The test vial in which the sensor is placed is filled with fluids of varying viscosity to represent viscosity shifts that precede sludge accumulation. Viscosities spanning those of bile with varying sludge content are from 1-14 cP. The viscosity of the test fluid was varied from 0 to 12 cP by first testing in air and then adding measured amounts of sucrose to DI water. For a run of this test, a 37.5x2 mm^2 sensor – biased by twelve neodymium magnets – was integrated with the stent. The resonant frequency of the magnetoelastic sensors typically shifted by a total of about 1.7 kHz (Fig. 8). This demonstrates sensitivity to viscosity shifts that precede tissue growth.

To simulate the mass loading effects of sludge accumulation, the medial surface of the sensor was coated with successive layers of paraffin. Typical results from a 37.5x2 mm^2 sensor biased by twelve neodymium magnets are shown in Figure 9. The resonant frequency shifts by 24 kHz after a mass of 45 mg has been added, in very good agreement with the updated theoretical model.

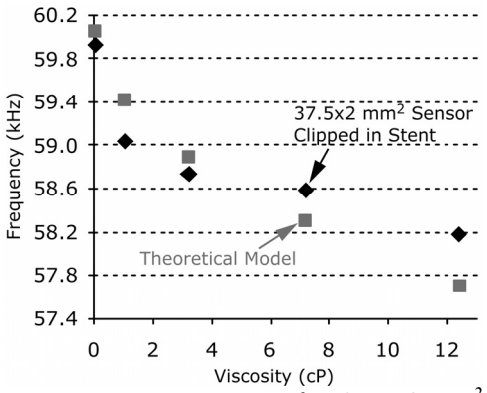

Fig. 8: Frequency v. viscosity for 37.5x2 mm^2 sensor clipped in stent with integrated magnets. The model uses an apparent modulus of 160.25 GPa.

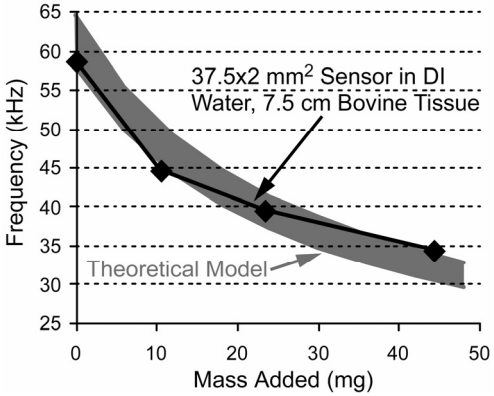

Fig. 9: Frequency vs mass loading for the sensor immersed in DI water (1 cP). The uncertainty in the model is due to uncertainty in E_o and ϕ in Eq. (1).

Because the exact location of the interrogation equipment with respect to the sensor can vary on a test-to-test or patient-to-patient basis, it is important to characterize the robustness of the signal as this relative location is varied. Figure 10 shows the variation in signal amplitude as the sensor position with respect to the interrogation equipment is varied. A symmetric

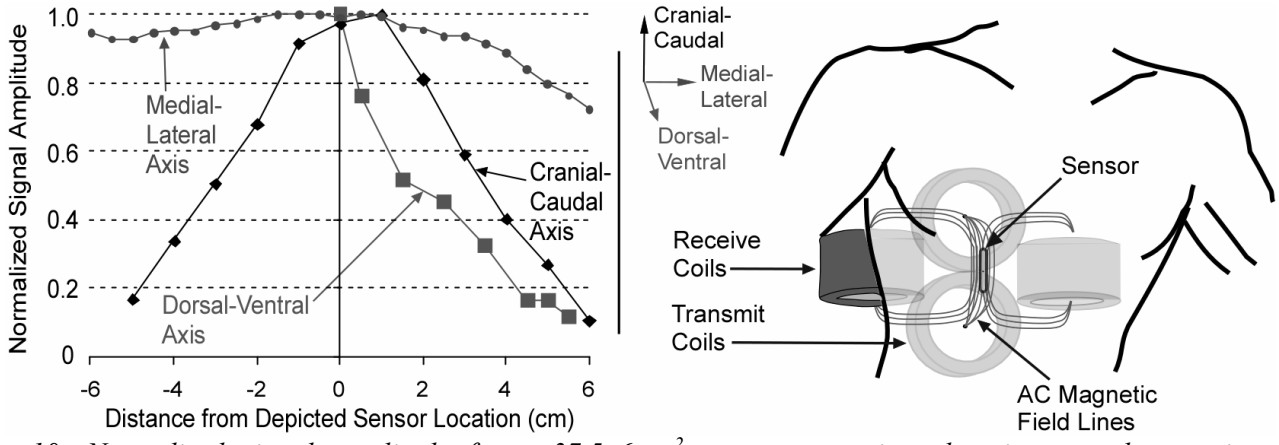

Fig. 10: Normalized signal amplitude for a 37.5x6mm^2 sensor at various locations to characterize coil performance. Perpendicular axis points into the body. The cranial-caudal axis range can be increased by separating transmit coils while boosting signal amplitude and using shorter sensors.

decrease in the signal amplitude is found when the sensor is moved in the cranial-caudal direction, with at least 80% of the signal still available with an offset of up to +/- 2 cm. Movement of the sensor in the medial-lateral direction resulted in a wider yet somewhat less symmetric signal magnitude distribution; at least 80% of the signal is still available with an offset of up to +/- 5 cm. Finally, movement in the posterior-anterior direction – which equates to movement closer to or farther from the coils – approximately shows the expected inverse cubic relationship between signal strength and distance. At least 80% of the signal is still available if the sensor is located 0.5 cm (in addition to the standard test setup of 7.5 cm) deeper into the tissue. The measured resonant frequency shifts only by approximately 0.3% over this entire range.

V. DISCUSSION

Though this work addresses one of the possible sources of error in this monitoring method and explores some of the potential in batch fabrication of biliary stents, further improvements are under investigation. This work utilized stents fabricated from 316L stainless steel; it was found during testing that the elastic recovery of this stent material – on the order of 2% – is well below that required for self-expanding biliary stents. This issue can be addressed by using a material with higher yield strength, such as Elgiloy, as well as adding stress-relieving features in the stent mesh.

The adhesive bond between the permanent magnets and the stent may be prone to failure. Also, as previously discussed, the rare-earth magnets need a parylene coating for protection against corrosion. Both of these weaknesses could potentially be avoided by depositing a thin film of Pt-Co on the stent, which can subsequently be magnetized [10]. This material has shown excellent resistance to corrosion [11].

VI. CONCLUSION

Batch fabricated planar biliary stents allow for integration of magnetoelastic sensors and permanent magnets for wireless monitoring of direct indicators of restenosis. Paraffin mass loads up to 45 mg simulated tissue growth on 37.5x2 mm^2, 28 μm thick sensors, resulting in a 24 kHz resonant frequency shift. As viscosity is varied from that of healthy bile to that of diseased bile, a resonant frequency shift of 1.7 kHz was measured. Appropriate scaling of this sensing methodology could allow use in stents of all kinds.

Acknowledgements: The authors acknowledge Dr. Grace Elta and Dr. Richard Kwon for discussions regarding stent usage. Metglas Inc. provided samples for this project. This work was supported in part by a NSF Graduate Research Fellowship, the NSF ERC for Wireless Integrated Microsystems (WIMS), and the University of Michigan.

[1] J.J.Y. Sung, S.C.S. Chung, "Endoscopic Stenting for Palliation of Malignant Obstruction: A Review of Progress in the Last 15 Years," Dig. Dis. and Sci., V. 40, No. 6 (June 1995), pp. 1167-1173.

[2] M.T. Richardson, S.R. Green, Y.B. Gianchandani, "Magnetoelastic Wireless Sensing of Tissue Growth for Self-Expanding Biliary Stents," IEEE MEMS 2007, pp. 469-472.

[3] K. Takahata et al., "A Wireless Microsensor for Monitoring Flow and Pressure in a Blood Vessel Utilizing a Dual-Inductor Antenna Stent and Two Pressure Sensors," IEEE MEMS 2004, pp. 216-219.

[4] M. Wilson et al., "Corrosion of intra-oral magnets in the presence and absence of biofilms of Streptococcus sanguis," Biomaterials, 16 (1995), pp. 721-725.

[5] L. Bondemark, J. Kurol, A. Larsson, "Long-term effects of orthodontic magnets on human buccal mucosa – a clinical, histological and immunohistochemical study," European J. of Orthod., 20 (1998), pp. 211-218.

[6] C. Grimes et al., "Magnetoelastic Microsensors for Environmental Monitoring," IEEE Transducers 2001, pp. 278-281.

[7] K. Takahata, Y.B. Gianchandani, "Batch Mode Micro-Electro-Discharge Machining," JMEMS, 11(2), April 2002, pp. 102-110.

[8] M. Dapino et. al., "A Model for the □E Effect in Magnetostrictive Transducers," Smart Struc. and Mat.: Proc. of SPIE Vol. 3985 (2000), pp. 174-185.

[9] P. Anderson III, "Magnetomechanical coupling, DE effect, and permeability in FeSiB and FeNiMoB alloys," J. Appl. Phys., 53(11), Nov. 1982, pp. 8101-8103.

[10] J. Aboaf, S. Herd, and E. Klokholm, "Magnetic Properties and Structure of Cobalt-Platinum Thin Films," IEEE Trans. on Magnetics, Vol. MAG-19, No. 4, July 1983, pp. 1514-1519.

[11] J.Driller, V. Parsonnet, "Magnetic Materials as Biological Implants – Criteria for Selection," IEEE Trans. on Magnetics, Vol. MAG-9, No. 3, Sept. 1973, pp. 444-447.